Reflectance confocal endomicroscope with optical axial scanning for *in vivo* imaging of the oral mucosa

Joey M. Jabbour,[1] Julie L. Bentley,[2] Bilal H. Malik,[1] John Nemechek,[3] John Warda,[4] Rodrigo Cuenca,[1] Shuna Cheng,[1] Javier A. Jo,[1] and Kristen C. Maitland[1*]

[1]*Department of Biomedical Engineering, Texas A&M University, 5045 Emerging Technologies Building, 3120 TAMU, College Station, Texas 77843, USA*
[2]*The Institute of Optics, University of Rochester, 275 Hutchison Road, Rochester, New York 14620, USA*
[3]*Metrology Concepts LLC., 3495 Winton Place, Bldg E-120, Rochester, New York 14623, USA*
[4]*Optics Technology Inc., 3800 Monroe Avenue, Suite # 6, Pittsford, New York 14534, USA*
[*]*kmaitland@tamu.edu*

Abstract: This paper presents the design and evaluation of a reflectance confocal laser endomicroscope using a miniature objective lens within a rigid probe in conjunction with an electrically tunable lens for axial scanning. The miniature lens was characterized alone as well as in the endoscope across a 200 µm axial scan range using the tunable lens. The ability of the confocal endoscope to probe the human oral cavity is demonstrated by imaging of the oral mucosa *in vivo*. The results indicate that reflectance confocal endomicroscopy has the potential to be used in a clinical setting and guide diagnostic evaluation of biological tissue.

OCIS codes: (220.3620) Lens system design; (350.3950) Micro-optics; (170.1790) Confocal microscopy; (170.2150) Endoscopic imaging; (120.3890) Medical optics instrumentation; (170.3880) Medical and biological imaging.

References and links

1. J. M. Jabbour, M. A. Saldua, J. N. Bixler, and K. C. Maitland, "Confocal endomicroscopy: instrumentation and medical applications," Ann Biomed Eng **40**, 378-397 (2012).
2. J. B. Pawley, *Handbook of biological confocal microscopy* (Springer, New York, NY, 2006).
3. J. C. T. Braga, M. P. Macedo, C. Pinto, J. Duprat, M. D. Begnami, G. Pellacani, and G. G. Rezze, "Learning reflectance confocal microscopy of melanocytic skin lesions through histopathologic transversal sections," Plos One **8**, e81205 (2013).
4. http://www.caliberid.com/vivacam-Overview.html
5. S. Gonzalez, K. Swindells, M. Rajadhyaksha, and A. Torres, "Changing paradigms in dermatology: confocal microscopy in clinical and surgical dermatology," Clinics in Dermatology **21**, 359-369 (2003).
6. R. T. Kester, T. S. Tkaczyk, M. R. Descour, T. Christenson, and R. Richards-Kortum, "High numerical aperture microendoscope objective for a fiber confocal reflectance microscope," Opt Express **15**, 2409-2420 (2007).
7. K. Carlson, M. Chidley, K. B. Sung, M. Descour, A. Gillenwater, M. Follen, and R. Richards-Kortum, "In vivo fiber-optic confocal reflectance microscope with an injection-molded plastic miniature objective lens," Applied Optics **44**, 1792-1797 (2005).
8. M. Kyrish, U. Utzinger, M. R. Descour, B. K. Baggett, and T. S. Tkaczyk, "Ultra-slim plastic endomicroscope objective for non-linear microscopy," Opt Express **19**, 7603-7615 (2011).
9. R. P. J. Barretto, B. Messerschmidt, and M. J. Schnitzer, "In vivo fluorescence imaging with high-resolution microlenses," Nat Methods **6**, 511-U561 (2009).
10. D. T. Moore, "Gradient-index optics - a review," Applied Optics **19**, 1035-1038 (1980).
11. J. K. Kim, W. M. Lee, P. Kim, M. Choi, K. Jung, S. Kim, and S. H. Yun, "Fabrication and operation of GRIN probes for in vivo fluorescence cellular imaging of internal organs in small animals," Nat Protoc **7**, 1456-1469 (2012).
12. J. Knittel, L. Schnieder, G. Buess, B. Messerschmidt, and T. Possner, "Endoscope-compatible confocal microscope using a gradient index-lens system," Opt Commun **188**, 267-273 (2001).
13. J. C. Jung, A. D. Mehta, E. Aksay, R. Stepnoski, and M. J. Schnitzer, "In vivo mammalian brain imaging using one- and two-photon fluorescence microendoscopy," J Neurophysiol **92**, 3121-3133 (2004).

14. B. F. Grewe, D. Langer, H. Kasper, B. M. Kampa, and F. Helmchen, "High-speed in vivo calcium imaging reveals neuronal network activity with near-millisecond precision," Nat Methods **7**, 399-405 (2010).
15. J. M. Jabbour, S. N. Cheng, B. H. Malik, R. Cuenca, J. A. Jo, J. Wright, Y. S. L. Cheng, and K. C. Maitland, "Fluorescence lifetime imaging and reflectance confocal microscopy for multiscale imaging of oral precancer," J Biomed Opt **18** (2013).
16. K. B. Sung, C. N. Liang, M. Descour, T. Collier, M. Follen, and R. Richards-Kortum, "Fiber-optic confocal reflectance microscope with miniature objective for in vivo imaging of human tissues," IEEE T Bio-Med Eng **49**, 1168-1172 (2002).
17. C. Olsovsky, R. Shelton, O. Carrasco-Zevallos, B. E. Applegate, and K. C. Maitland, "Chromatic confocal microscopy for multi-depth imaging of epithelial tissue," Biomed Opt Express **4**, 732-740 (2013).
18. E. J. Botcherby, R. Juskaitis, M. J. Booth, and T. Wilson, "Aberration-free optical refocusing in high numerical aperture microscopy," Opt Lett **32**, 2007-2009 (2007).
19. B. F. Grewe, F. F. Voigt, M. van 't Hoff, and F. Helmchen, "Fast two-layer two-photon imaging of neuronal cell populations using an electrically tunable lens," Biomed Opt Express **2**, 2035-2046 (2011).
20. J. M. Jabbour, B. H. Malik, C. Olsovsky, R. Cuenca, S. N. Cheng, J. A. Jo, Y. S. L. Cheng, J. M. Wright, and K. C. Maitland, "Optical axial scanning in confocal microscopy using an electrically tunable lens," Biomed Opt Express **5**, 645-652 (2014).
21. R. A. Drezek, T. Collier, C. K. Brookner, A. Malpica, R. Lotan, R. R. Richards-Kortum, and M. Follen, "Laser scanning confocal microscopy of cervical tissue before and after application of acetic acid," Am J Obstet Gynecol **182**, 1135-1139 (2000).
22. M. C. Skala, J. M. Squirrell, K. M. Vrotsos, V. C. Eickhoff, A. Gendron-Fitzpatrick, K. W. Eliceiri, and N. Ramanujam, "Multiphoton microscopy of endogenous fluorescence differentiates normal, precancerous, and cancerous squamous epithelial tissues," Cancer Res **65**, 1180-1186 (2005).
23. A. L. Clark, A. M. Gillenwater, T. G. Collier, R. Alizadeh-Naderi, A. K. El-Naggar, and R. R. Richards-Kortum, "Confocal microscopy for real-time detection of oral cavity neoplasia," Clin Cancer Res **9**, 4714-4721 (2003).

1. Introduction

The utility of reflectance confocal microscopy (RCM) is underscored by its ability to provide high fidelity, label-free cross-sectional images of biological tissue at sub-cellular resolution [1, 2]. It is a non-invasive technique that can provide information on cell and tissue microanatomy and has been shown to correlate well with more conventional histological analysis [3]. Its application in imaging of epithelial tissue is well researched and documented, and has resulted in commercially available RCM systems accepted by clinicians [4, 5].

Despite the aforementioned advantages, *in vivo* applications of RCM have been somewhat limited, mainly due to the constraints put forth by the bulk of optics, particularly in high resolution systems. Toward this end, miniaturization of the microscope objective is arguably the most important step in realization of practical, compact and mobile reflectance confocal laser endomicroscopy (rCLE) systems. Development in this area has mainly been in two categories: multiple-lens objectives and probes based on graded-index (GRIN) lenses. Multiple lens objectives can offer high numerical aperture (NA) while minimizing aberrations, all at diameters of a few millimeters. Such microscope objectives have been used in rCLE systems [6, 7], as well as other high resolution imaging modalities such as non-linear microscopy [8, 9]. On the other hand, GRIN based objectives and probes can provide the smallest diameters, low cost and ease of assembly at the expense of inherent aberrations due to the non-aplanatic nature of these rod lenses [10, 11], and have been utilized by multiple optical imaging techniques including rCLE [12, 13].

A major challenge with volumetric imaging *in vivo* is the ability to implement fast depth scanning. While 2D sampling rates have surpassed several hundreds of Hertz [14], scanning in the axial direction has not followed suit. More importantly, most realizations of axial scanning require moving the sample or the objective lens relative to each other, typically adding to the bulk of optics, and hence limiting the compactness and usability of the imaging system *in vivo* [15, 16]. To address this concern, a number of “optical axial scanning” mechanisms have been reported which allow for smaller footprint of the imaging system and are inherently less susceptible to motion artifact [17, 18]. More recently, electrically tunable lenses (ETL) have

been employed to vary the imaging depth within the sample [19, 20]. While these applications of ETL have demonstrated to be fast and relatively simple to implement, the proposed embodiments have been limited to 'bench-top' use in conjunction with relatively large microscope objectives.

In our continuing effort towards development of a compact and mobile rCLE system, we present a rigid handheld endomicroscope which addresses the two aforementioned limitations currently preventing the realization of practical rCLE systems. Specifically, we report a miniaturized multiple-lens microscope objective custom designed to be used with optical axial scanning using an ETL. The small size of the objective allows relatively easy access to the oral cavity, and along with ETL, can provide volumetric imaging of the oral mucosa *in vivo*, which is the ultimate application of our endoscope system. Nonetheless, the robustness and light-weight of the rigid probe can easily allow imaging of other diseases of the epithelium such as that of skin, cervix and rectum. The proof-of-concept demonstrates and enables the technique of rCLE for potential disease detection and diagnosis *in vivo*.

2. rCLE system

The CAD model of the complete system is shown in Figure 1. The rCLE system consists of a handheld box with a rigid tube 127mm in length and 6.4 mm in outer diameter at the tip. The light source and detector are placed on a portable cart and fiber-coupled to the handheld unit. To exploit the enhanced penetration depth of near infrared light in tissue due to lower scattering and absorption, an 807 nm continuous wave laser (DL808-120-0, Crystalaser) beam is delivered by a 10 µm core diameter polarization maintaining single mode fiber (P1-780PM-FC-2, Thorlabs) connected to a 12.2 mm focal length fiber collimator (TC12FC-780, Thorlabs). The laser beam is raster scanned by two closely spaced scanning mirrors (CRS 8 KHz resonant scanner and 6200H galvanometer scanner, Cambridge Technology). A 2× beam expander (AC127-025-B-ML and AC127-050-B-ML, Thorlabs) forms the rigid endoscopic tube and relays the mid plane between the two scanning mirrors onto the back focal plane of a custom miniature objective lens.

An electrically tunable lens (ETL, EL-6-18, Optotune) is positioned close to the scanning mirrors, near the image of the back focal plane of the objective lens. An ETL control current of 50 mA corresponds to a focal length of infinity. Increased current results in increased convex lens curvature, and decreased current below 50 mA results in increased concave lens curvature. By adjusting the focus of the ETL, the focal plane of the microscope is axially scanned within the sample [19]. This obviates the need for an axial scanning mechanism at the distal end of the imaging probe.

In combination with a quarter wave plate (AQWP05M-980, Thorlabs) placed before the objective lens, a polarizing beam splitter cube (PBS102, Thorlabs) separates the illumination from the reflected light. In the detection arm, a polarizer (LPNIR050-MP2, Thorlabs) removes specular reflections, followed by light collection and spatial filtering by a 11 mm focal length fiber collimator (PAF-X-11-PC-B, Thorlabs) and 10 µm core diameter fiber (M64L02, Thorlabs) coupled to a photomultiplier tube (H9305-03, Hamamatsu Corporation). A digitizer (PXIe-5185, National Instruments) is used for voltage signal collection, digitization at 39.55 MHz and real-time corrected image formation at a frame rate of 7 Hz. A user friendly acquisition and instrument control software package has been developed using LabVIEW (National Instruments) to be used specifically in a clinical environment. The outer housing of the rCLE is made out of Delrin plastic, which is known for its robustness and light weight.

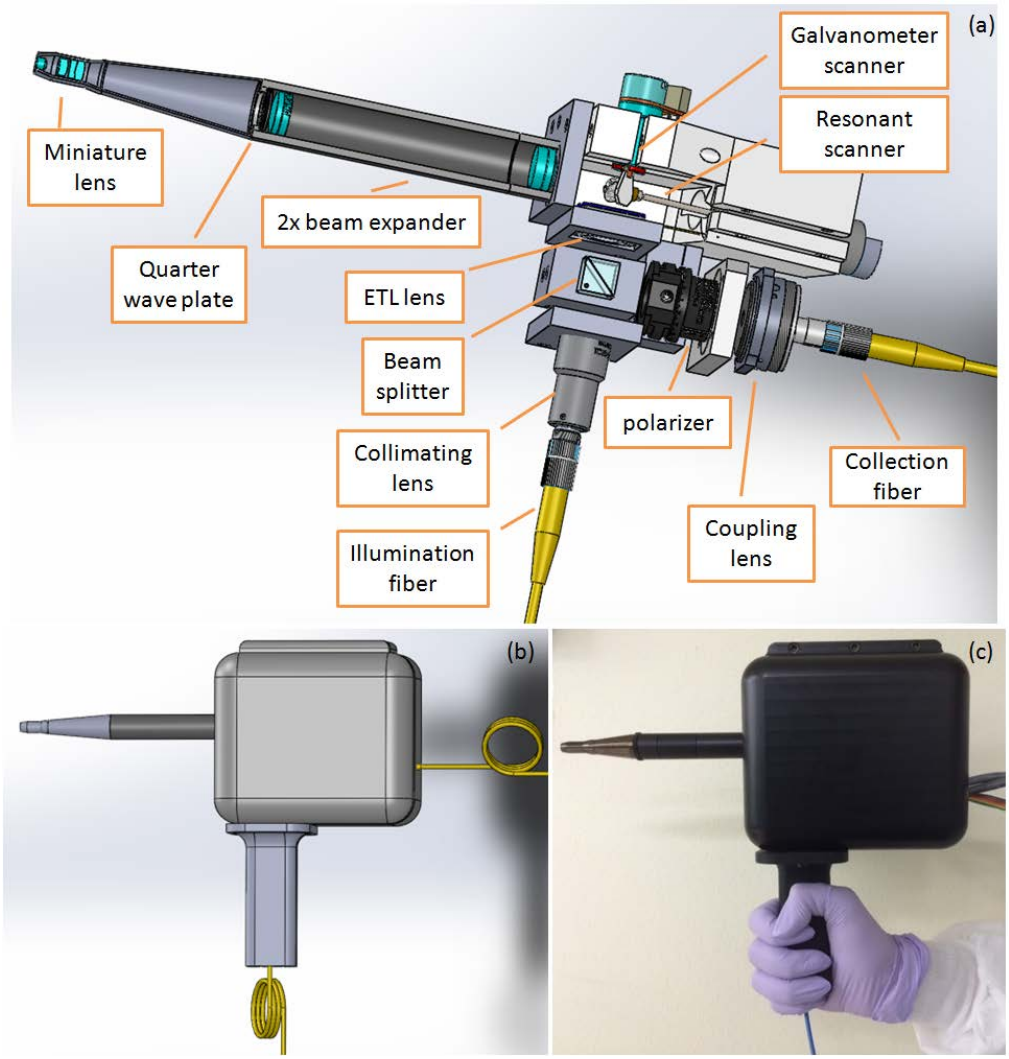

Fig. 1. (a) CAD model of the rCLE system illustrating the optical setup. (b) CAD model and (c) photo of the clinical handheld rCLE system.

3. Miniature lens design

Figure 2 shows the optical layout of the four-element miniature microscope objective lens. The lens was designed to be used with a wavelength of 811+/- 5 nm. It has an effective focal length of 5 mm and a back aperture diameter of 7 mm. The image plane of the objective is allowed to slightly curve to reduce the need for correcting Petzval field curvature, which in turn reduces the complexity and size of the objective (e.g. smaller element count). The image radius is 3.3 mm, corresponding to sag of 6.8 µm, which is slightly more than the axial resolution but less than the thickness of one cell layer within epithelial tissue. The nominal working distance of the objective lens, when used as an infinity objective, is 305 µm outside the flat surface of the last lens. This working distance serves to provide sufficient penetration of light in the tissue, while allowing the lens to be placed in contact with the sample to reduce motion artifacts during imaging. In addition, since the objective is used in contact with tissue, it is designed to be a water-immersion objective, with a nominal NA of 0.7 in water (n=1.33). The large NA enables the microscope objective to maximize collection of light reflected from

the tissue. As the effective focal length of the ETL lens varies from -127.0 mm (0 mA) through infinity (50 mA) to +44.3 mm (200 mA), the light entering the objective lens changes in divergence and beam diameter. This results in a shift in the working distance and NA of the lens at the tissue space. With 4 degrees scan angle entering the objective lens, the paraxial image height equivalent to half field of view (FOV) is 350 μm at the nominal working distance, sufficient for imaging epithelial cells. Table 2 lists the curvatures of the optical surfaces and glass materials of the lenses. Figure 3 shows the performance of the infinity-corrected objective lens at nominal working distance: the field curvature and distortion within the FOV, the RMS wavefront error showing diffraction limited performance across the different fields, and the modulation transfer plots.

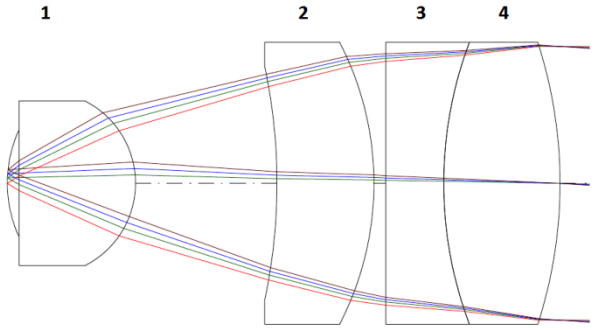

Fig. 2. Optical design of the miniature objective lens.

Table 2. Miniature objective lens prescription. CX: Convex, CC: Concave, L: Lens, S: Surface.

Element	Radius of Curvature (mm)	Thickness (mm)	Lens Diameter (mm)	Glass
Object	3.269 CX	0.305	-	'water'
L1 S1	Infinity	3.000	4.2	NLAK10
L1 S2	2.350 CX	3.649	-	
L2 S1	14.220 CC	2.500	7.2	NLAK12
L2 S2	7.783 CX	0.300	-	
L3 S1	Infinity	1.500	7.2	NSF4
L3 S2/L4 S1	10.147 CC	3.000	7.2	NSK14
L4 S2	11.592 CX	0.000	-	
Stop/Image	Infinity	Infinity	7.0	

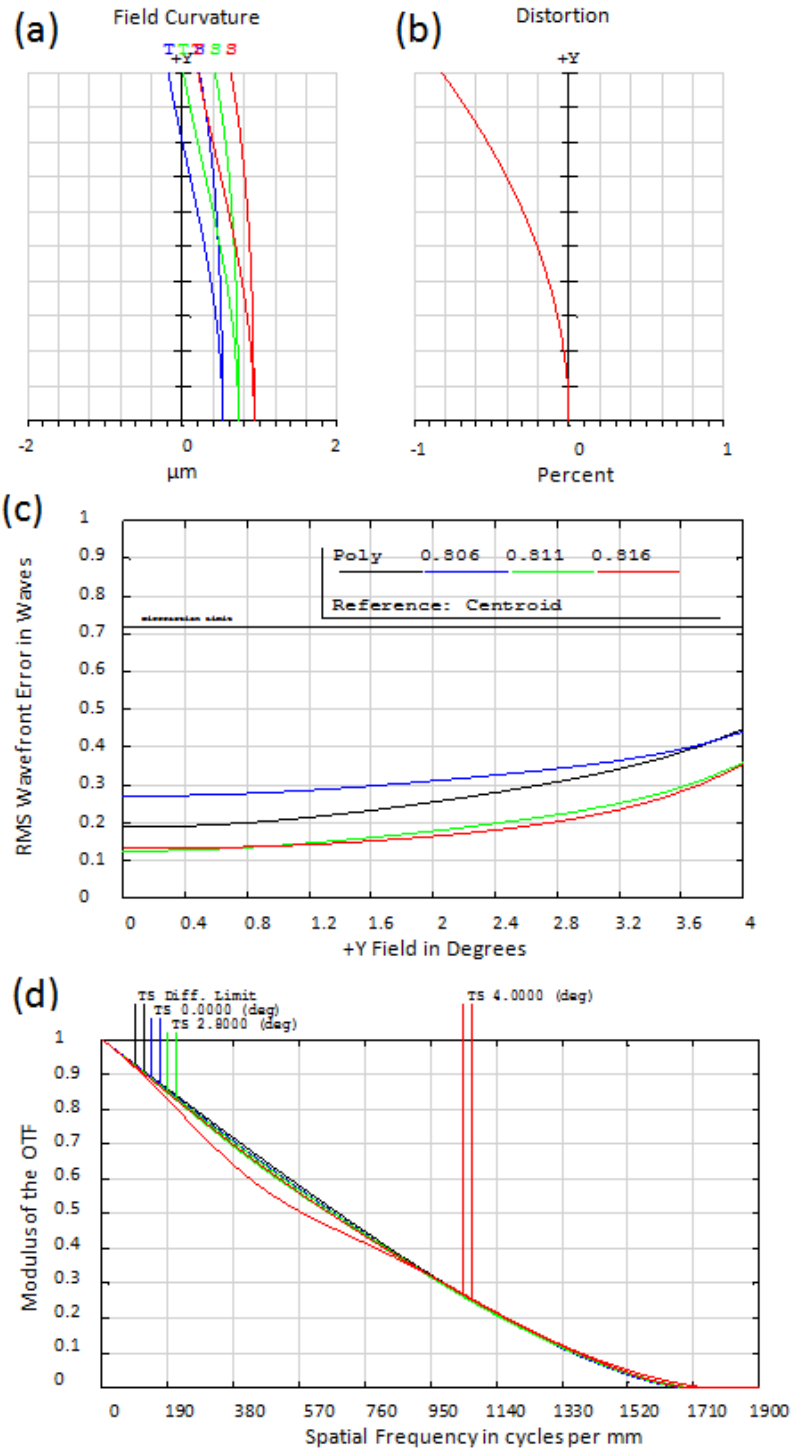

Fig. 3. (a) Field curvature and (b) distortion of the miniature objective lens design for wavelengths of 0.806 µm (blue), 0.811 µm (green), and 0.816 µm (red). Maximum field is 4 degrees. (c) RMS wavefront error across field. (d) Polychromatic diffraction modulation transfer function of the miniature objective lens design for the fields above and for wavelengths from 0.806 to 0.816 µm.

4. Miniature lens manufacturing, assembly and testing

The lens elements were fabricated at Optics Technology Inc., coated at Accucoat Inc., and measured for wavefront performance at Metrology Concepts. All optical surfaces, except cemented surfaces on lenses 3 and 4, are coated with anti-reflection coatings to reduce reflectance to <0.2% at 0 degrees and <0.3% at 40 degrees. Optical elements are encased in a stainless steel mechanical housing with black nickel plating. The 20 mm long objective was designed to be as compact as possible, particularly at the probe tip, to allow access into the oral cavity and improve accuracy of probe placement. The barrel outer diameter is 6.5 mm at the surface in contact with tissue, 8.2 mm for the main barrel, and flared to 10 mm at the proximal end. Figure 4 shows photographs and Table 3 lists the fabrication tolerances of the miniature objective lens. The expected as-built performance with this set of tolerances is <0.05 wave root mean square (RMS) for an axial object point and <0.06 wave RMS for a full field object point at 98% yield.

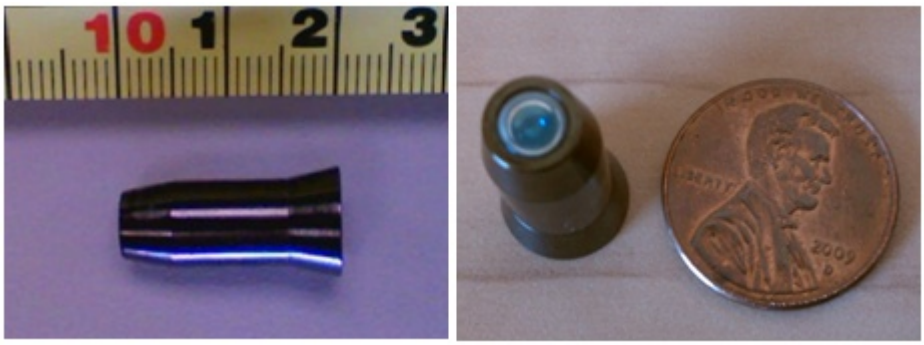

Fig. 4. Photographs showing the assembled miniature objective next to a ruler and a United States penny.

Table 3. Lens system tolerances for miniature lens design

Radius (mm)	Thickness/ Airspace (mm)	Irregularity (fringe)	Wedge (mm TIR)	Element Decenter (mm)	Element Tilt (mrad)
±0.025	±0.005 - 0.025	0.25-0.5	0.008 - 0.010	±0.020	±1

The as-built objective lens was evaluated using a Twyman Green interferometer. As shown in Figure 5, the objective lens was illuminated with a collimated wavefront that was retro-reflected back through the objective by means of a high quality reference sphere. The cavity between the objective and retro sphere was filled with water (refractive index of 1.33). The interference pattern formed at the beam splitter was imaged onto a camera. The wavefront quality of the miniature objective was assessed by means of phase-shifting, whereby several camera frames of interference fringe patterns were collected after a controlled phase-step of the reference arm using a piezo-electric device. In this manner, fringe intensity information is converted to a phase map of the aberrations present in the pupil of the lens under test.

Figure 6 shows the measured on-axis RMS wavefront performance to be 0.042 (well within the 98% yield target of 0.05 wave RMS). While we tested the lens outside of the design wavelength range (785 nm), this is acceptable since the lens can compensate for this slight deviation with a small change in the back focal distance. The magnitude of wavefront error is often reported in terms of peak to valley (PV) and/or RMS. A practical definition of a “diffraction limited” lens is often considered for lenses with PV results of a quarter-wave or RMS results of a twentieth of a wave. Although the PV magnitude of wavefront error was measured to be 0.341, the RMS magnitude was 0.042. An RMS metric is often preferred as the more statistically reliable result as it utilizes all available data points; whereas PV relies on just two data points.

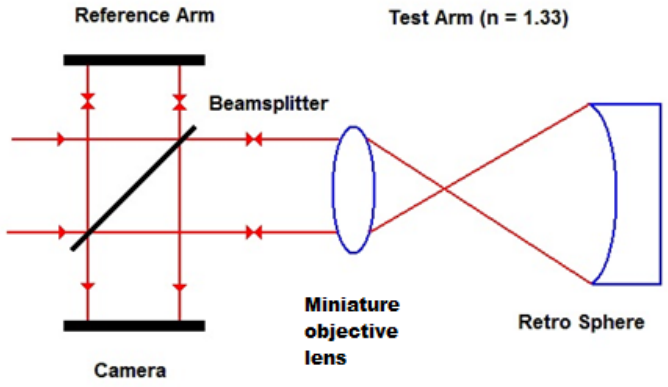

Fig. 5. Schematic diagram of the Twyman interferometry setup used for evaluation of the miniature objective lens.

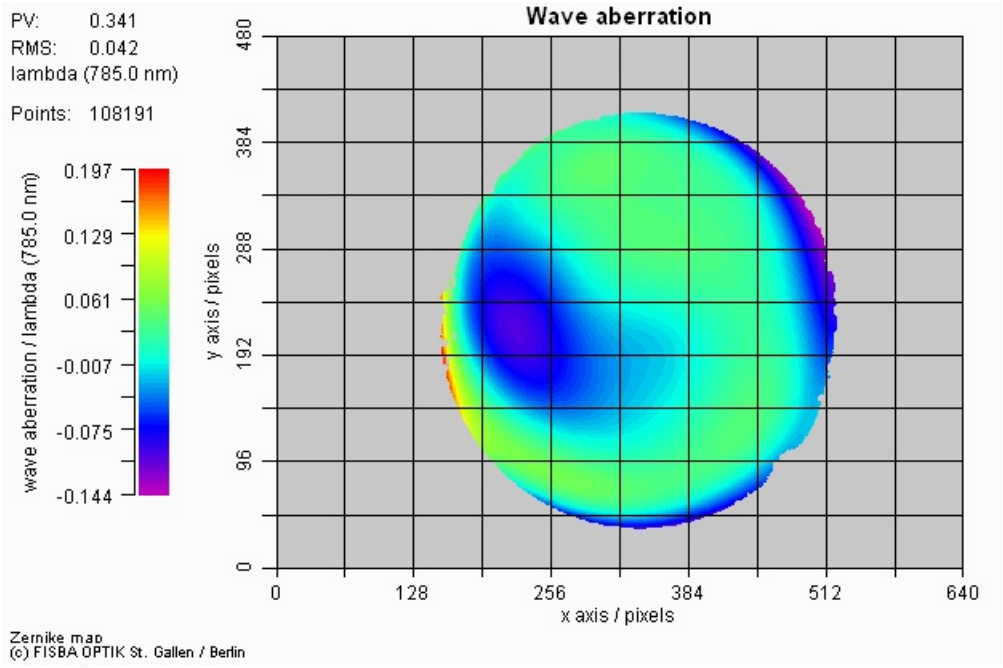

Fig.6. Zernike 2D plot showing the wave aberration of the miniature objective lens.

5. Imaging performance of the rCLE system

The imaging performance specifications of the rCLE system with miniature lens and optical axial scanning are summarized in Table 4. To test the axial scan range of the system with ETL scanning, a mirror was placed on a motorized stage and the relative position of best focus was recorded across the full range of ETL control current. The measured axial scan range was 200 µm as the control current was varied from 0 to 200 mA. This scan range is appropriate for imaging cellular changes within the epithelium, within the constraints of penetration of near infrared light into tissue.

Table 4. Imaging parameters as a function of current applied to the ETL

ETL Current (mA)	Relative Axial Position (μm)	Lateral Resolution (μm)	Axial Resolution (μm)
0	200	1.4	5.0
25	165	1.6	6.0
50	135	1.7	6.7
75	95	1.7	6.9
100	95	1.9	7.5
125	75	1.6	8.0
150	35	1.8	8.7
175	15	1.8	9.0
200	0	1.9	11.0

The lateral and axial resolutions were measured across the full range of the ETL control current. Lateral resolution was first evaluated qualitatively by imaging elements of groups 7, 8 and 9 of the high resolution 1951 U.S. Air Force resolution target. As seen in Figure 7(b), element 6 of group 8 (456.1 line pairs/mm, 1.1 μm line width) was clearly resolved. Quantitatively, the lateral resolution was calculated by taking the derivative of the edge-spread function, fitting it to a Gaussian function, and measuring the full width half maximum (FWHM) of the Gaussian curve [20]. The measured lateral resolution ranges from 1.4 to 1.9 μm over the axial scan range.

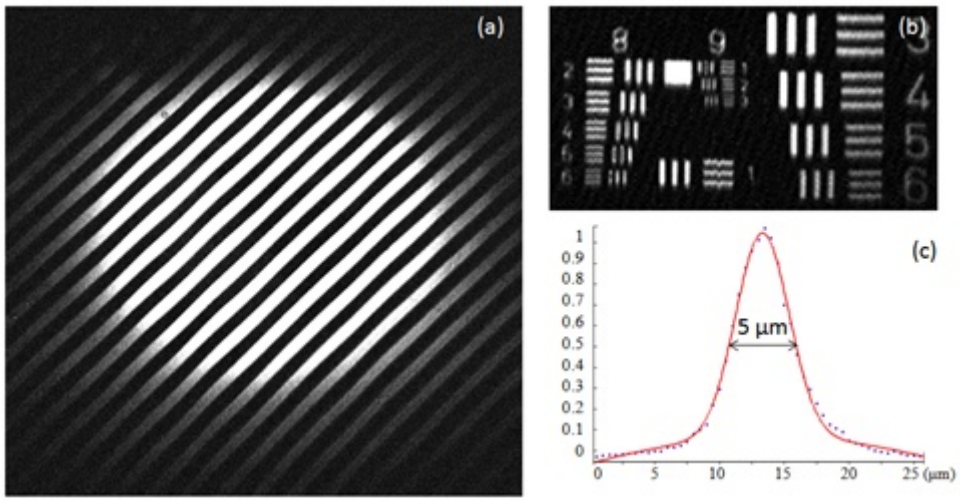

Fig.7. (a) Ronchi ruling showing 550 μm FOV of the rCLE with miniature objective lens. (b) Groups 8, 9 and 7 (to the right) of USAF target at 0 mA ETL current. (c) Axial resolution plot showing a FWHM of 5 μm at 0 mA ETL current.

Axial resolution was measured by translating a planar mirror axially in steps of 0.5 μm and measuring the FWHM of the Gaussian fit of the recorded intensity plot (Figure 7(c)). The axial resolution varies from 5μm at the deepest focus to 11μm close to the surface. This change in resolution is expected with ETL scanning [20]. As the ETL's focal length varies from infinity to 60 mm, the beam diameter at the back aperture of the objective lens is reduced and the effective NA at the sample therefore decreases. For the purpose of cellular imaging within the epithelium, there is usually less crowding of cells and nuclei at superficial layers, and hence, the lower resolution is acceptable and adequate to resolve the microanatomical features therein.

To test the FOV, a Ronchi ruling of 40 line pairs/mm was imaged at the nominal working distance of the lens. A total of 22 line pairs were observed within the FOV, which is

equivalent to 550 µm across the center of the image (Figure 7(a)). The measured field of view is less than the 700 µm design specification because the scan angle is limited by the range of the scanning mirrors and slight clipping from the lens tube housing. Intensity drops off at the edge of the image in Figure 7(a) due to the field curvature and flat sample.

To demonstrate the practical performance of the miniature objective lens with ETL scanning, imaging of normal human oral mucosa of several volunteers was performed *in vivo*. The protocol was reviewed and approved by the Texas A&M University Institutional Review Board. Before imaging, a cotton pad soaked in 5% acetic acid was applied to the oral site to be imaged. Acetic acid is applied to increase contrast between the nuclei and the cytoplasm of epithelial cells in RCM [21]. The tip of the probe was gently placed in contact with the tissue. The epithelial tissue was scanned with the ETL at frequency of 0.2 Hz over an axial scan range of 200 µm across the ETL control current range of 0 to 200 mA. A 0.2 Hz ETL speed acquires 17 confocal images from different depths through 200 µm thick tissue. Changing the axial scanning speed is possible by varying the frequency of the control current to the ETL, thereby changing the number of images acquired per total axial scan range.

Figure 8 demonstrates the capability of the miniature lens to show sub-cellular epithelial features *in vivo*. Media 1 and Media 2 videos were acquired from the buccal mucosa and inner lip of human volunteers, respectively. Extracted images at multiple depths are shown along with zoomed in images showing features of interest. Bright nuclei (marked by arrows) in contrast with darker cytoplasmic regions could be seen throughout the scanned depth of the tissue. As hypothesized above, while the axial and lateral resolution were lower in the superficial region of the tissue, the system was still able to resolve sub-cellular features, further demonstrating the ability of our rCLE embodiment to characterize tissue *in vivo*.

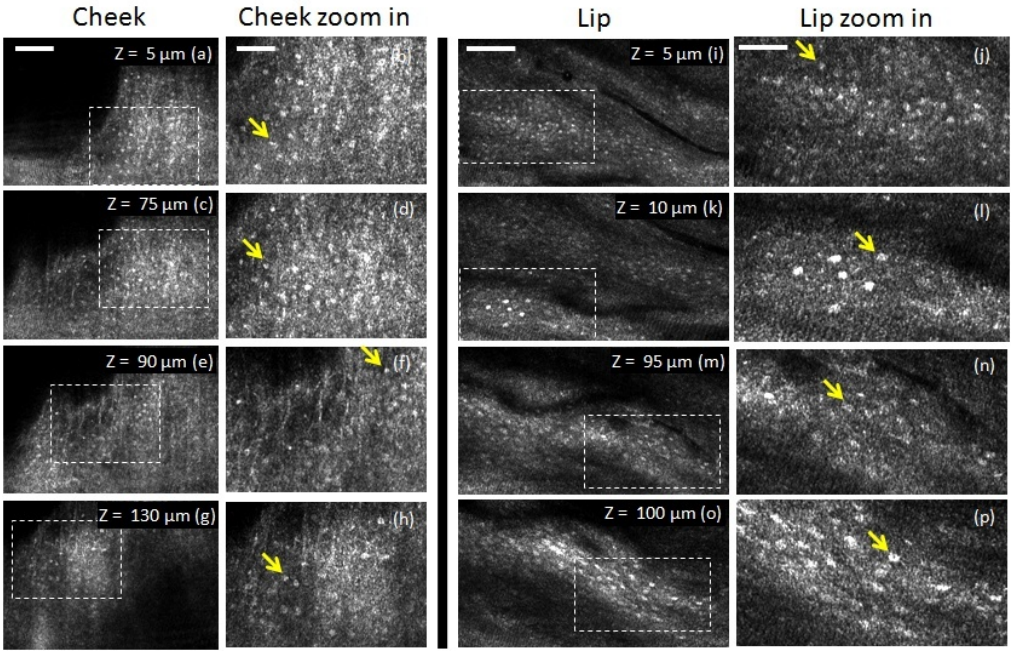

Fig. 8. rCLE images from human volunteers *in vivo* of (a-h, Media 1) buccal mucosa/cheek and (i-p, Media 2) inner lip tissue. (b,d,f,h) are zoomed in images from the corresponding dashed boxes in (a,c,e,g), and (j,l,n,p) are zoomed in images from the corresponding dashed boxes in (i,k,m,o), respectively. Arrows point to individual nuclei. Cell borders can be identified in (e,f). Scale bars: 100 µm in (a,i) and 50 µm in (b,j) for zoom in versions.

This work shows that our miniature objective lens design in combination with the optical scanning of the ETL can successfully enable rCLE to rapidly image morphological features of epithelial tissue at multiple depths *in vivo*. The bright nuclei observed across the full depth of

the tissues can be utilized to generate more objective parameters such as nuclear size and nuclear-to-cytoplasmic ratio, both of which have previously been observed to vary as a function of disease progression in epithelial tissue [22, 23].

As stated earlier, one of the ultimate goals of this study was to reduce the size of the imaging probe in order to provide better access to biological tissue *in vivo*. The ability to reach internal cavities and regions of the human body is exceedingly critical in order to realize the clinical potential of RCM *in vivo*. Our previous report demonstrating optical axial scanning using a tunable focus lens was a step towards the overall miniaturization of the system, by eliminating the complexity and bulk associated with mechanical scanning [20]. The integration of the optical scanning and the miniature objective lens reported here allows us to fully exploit the potential of rCLE, and we demonstrated the applicability through real-time imaging (Media 1 and Media 2) of multiple locations within the human oral cavity. Our results support the idea that rCLE can play a significant role in clinical evaluation of diseased lesions and/or monitoring of tissue response to therapy.

6. Conclusion

In summary, we have presented the design, development and testing of a new rCLE system with a miniature objective lens and ETL axial scanning for imaging of oral tissue *in vivo*. While the current miniature lens design is used with a focus tunable lens, the model would be applicable to other embodiments of rCLE with minimal modifications. Our future work includes the characterization of this system for detection of oral precancer *in vivo* in a clinical environment.

Acknowledgments

The authors would like to thank Drs. Yi-Shing Lisa Cheng and John M. Wright from the Department of Diagnostic Sciences at Texas A&M Health Science Center – Baylor College of Dentistry for their notable feedback in the design of the rCLE rigid probe system. The authors would also like to thank Ms. Fatemeh Nooshabadi and Ms. Madeleine Durkee from the Department of Biomedical Engineering at Texas A&M University for their help with *in vivo* imaging. This work was supported by the National Cancer Institute of the National Institutes of Health (R01 CA138653).